Dyes and Pigments xxx (xxxx) 110473

Contents lists available at ScienceDirect

Dyes and Pigments

journal homepage: www.elsevier.com/locate/dyepig

Polarized emission and mechanofluorochromism of benzothiadiazole based chromophores oriented by rubbing

Benedetta Maria Squeo [a], Fabio Bertini [a], Guido Scavia [a], Michela Uslenghi [b], Ettore S. Fois [c, **], Mariacecilia Pasini [a, ***], Chiara Botta [a, *]

[a] Istituto di Scienze e Tecnologie Chimiche "G. Natta" SCITEC, CNR, via A.Corti 12, 20133, Milano, Italy
[b] INAF/IASF-Milano, Via A. Corti 12, 20133, Milano, Italy
[c] Insubria University, DSAT, via Valleggio 11, I-22100, Como, Italy

A B S T R A C T

Mechanofluorochromic (MFC) organic chromophores are a versatile class of materials whose applications include mechanical sensors, security inks and optical data storage devices. Molecules with Liquid-Crystal (LC) properties can be easily oriented by several techniques providing films with highly anisotropic properties. Thin organic films with polarized emission properties rapresent ideal materials for OLED applications requiring polarized emission, such as backlights for commercial LC displays. We have synthetized molecules and polymers composed of a rod-like rigid core based on the highly emissive benzothiadiazole moiety and flexible chains to produce oriented films with polarized emission in the green/yellow and red regions. Films oriented by mechanical rubbing display absorption anisotropies and emission polarization up to 5. Beside orienting the molecular axis of the molecules, mechanical rubbing induces a conformational relaxation towards their most stable and elongated state thanks to the arrangement of the terminal alcoxy chains. According to the chromophore molecular structure, the oriented films display either stable (polymers) or mechano-sensitive (molecules) polarized emissions with fluorescence efficiencies up to 1. In the molecular blends highly sensitive polarized MCF, originating from the peculiar modulation of the energy transfer efficiency directly in bulk, opens to smart sensors able to detect the direction of application of a mechanical stress.

1. Introduction

The availability of thin films with bright polarized emission is particularly desired in view of many application fields, going from energy saving liquid-crystal display technologies [1–3] to linearly polarized luminescent solar concentrators with broad absorption across the visible [4]. A low–cost and extremely efficient strategy to fabricate thin films able to emit polarized light is to orient linear chain organic dyes that possess intrinsic anisotropy, in both absorption and emission, thanks to the alignment of their molecular transition moment along the molecular axis. The molecular anisotropy of the dye's conjugated backbones is then transferred to the macroscopic scale by orientation of the dyes deposited onto a substrate. Since molecules possessing Liquid-Crystal (LC) properties can be easily oriented by several standard procedures [5–7], films of oriented emissive molecules are generally prepared by blending them with LC hosts [5,8]. In some cases bulk films of emissive conjugated molecules or polymers can be oriented by a mechanical force, such as rubbing [7,9,10], without the need of pre-aligned substrates. Following this strategy oriented thin films of organic materials that generally possess LC properties have been prepared and successfully used as active materials in OLED with polarized electroluminescence [11,12].

One of the strategies proposed in order to obtain organic materials that can be oriented and with outstanding absorption and emission properties is the development of molecules composed of a rod-like rigid linear conjugated core and flexible linear alkyl chains at the terminal [13–16]. The core imparts the optical characteristics (absorption and emission) of the material while the alkyl chains can be oriented by a mechanical force, such as rubbing, creating short wires in the rubbing direction that lead to a polarized luminescence and, in some cases, to stimuli-responsive luminescence [17–19]. Emissive systems able to change their emissive properties (intensity and colour) upon a mechanical stress represent the intriguing class of Mechanofluorochromic (MFC) materials.

The interest in MFC organic materials has been considerably increasing in the last years because of their attractive optical characteristics and for the variety of applications of these materials including mechanical sensors, security inks and optical data storage devices

* Corresponding author.
** Corresponding author.
*** Corresponding author.
E-mail addresses: ettore.fois@uninsubria.it (E.S. Fois), mariacecilia.pasini@scitec.cnr.it (M. Pasini), chiara.botta@scitec.cnr.it (C. Botta).

https://doi.org/10.1016/j.dyepig.2022.110473
Received 25 March 2022; Received in revised form 1 June 2022; Accepted 1 June 2022
0143-7208/

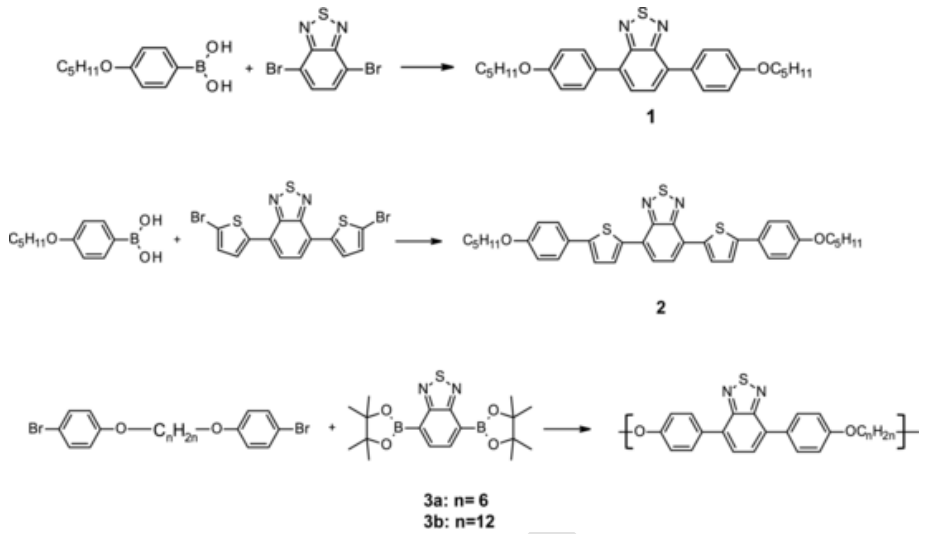

Scheme 1. Chemical structure of molecules **1**, **2** and polymers **3**.

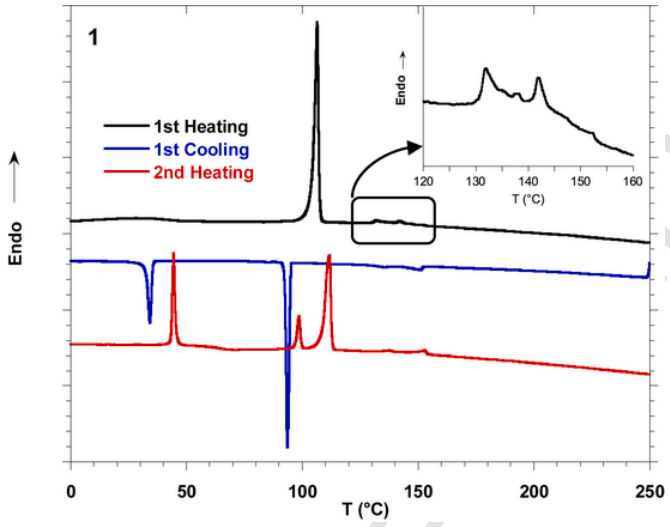

Fig. 1. DSC traces of **1** recorded at 10 °C/min: heating run of the pristine material (black line); successive cooling run (blue line); second heating run (red line). In the inset an enlargement of the 120–160 °C range is shown for the first heating run.

[19–21]. MFC materials change their emission colour and/or intensity under external mechanical stimuli such as pressing, grinding, crushing or rubbing. In some cases, their pristine properties can be restored by thermal treatments or solvent fuming, making the MCL process reversible for many cycles. The MFC mechanism of organic materials originates from the facile modification of the weak intermolecular interactions that impose their molecular packing modes [21–24]. In fact, the emissive properties of molecular organic materials are strictly correlated to their intra- and inter-molecular interactions. Generally, MFC involves transitions from the crystalline to the amorphous state or between two different crystalline states of the chromophores [22–24]. In some cases they display MCF properties and represent optimal materials for mechanical sensing [13,25]. Ideally, by using this class of materials, smart sensors capable to identify the direction of application of the mechanical force can be envisaged.

With this in mind we design and synthesize molecular systems with LC properties based on the highly emissive benzothiadiazole moiety [8,25–27], whose mechano-responsive properties have already been reported [28–30]. In this work we further optimize the molecular approach by proposing the use of poly(rod-coil) polymers to improve the morphological stability of the oriented films. In fact, the rod coil polymer approach, consisting in conjugated rod segments interconnected with coil alkyl chains, has been recently proposed for photovoltaics application proving to be particularly effective for controlling the morphology of materials [31–34].

2. Methods

2.1. Materials

All reagents were purchased from commercial source Aldrich and TCI) and used without further purification. Toluene was freshly distilled prior to use according to literature procedure. All reactions were carried out in inert atmosphere. Synthetic procedures and chemical characterizations are reported in SI. The films, deposited by spin-coating (4000 rpm) from 20 to 25 mg/ml chloroform or DCM solutions onto silica substrates, are oriented by mechanical rubbing with a velvet cloth in order to align the rod-chain molecules along the rubbing direction. The mechanical orientation of the films is performed with a rubbing machine (Fig. S9) by varying the cumulative number of rubs from 2 to 5 and the pile impression of the velvet fibres in order to obtain the best film anisotropy combined with absorbance >0.2. The roller radius is 6 cm, the rotation speed of the roller was fixed at 200 rpm and the translational speed at 1 cm/s.

The molecular weight distribution (MWD) measurements were performed by using an integrated GPCV2000 SEC system from Waters equipped on-line with a differential refractometer as concentration detector. Measurements have been carried out in o-dichlorobenzene at 135 °C using Polystyrene standards. Differential scanning calorimetry (DSC) analysis was carried out under nitrogen flow using a PerkinElmer DSC 8000 calorimeter. The sample was heated from −20 to 250 °C at a rate of 10 °C/min and kept at 250 °C for 3 min to erase previous thermal history; then it was cooled to −20 °C at 10 °C/min and subsequently heated with the same rate up to 250 °C. Thermogravimetric analysis (TGA) was carried out on a PerkinElmer TGA 7 analyzer. The sample was heated from 50 to 700 °C under nitrogen atmosphere at a constant heating rate of 20 °C/min, then kept at 700 °C for 10 min under air atmosphere.

2.2. Spectroscopic methods

UV–Vis absorption is performed with a Lambda900 PerkinElmer spectrometer. Extinction molar coefficients of 24340 $Lmol^{-1}cm^{-1}$ for **1** and 18400 $Lmol^{-1}cm^{-1}$for **2** have been measured in DCM solutions at

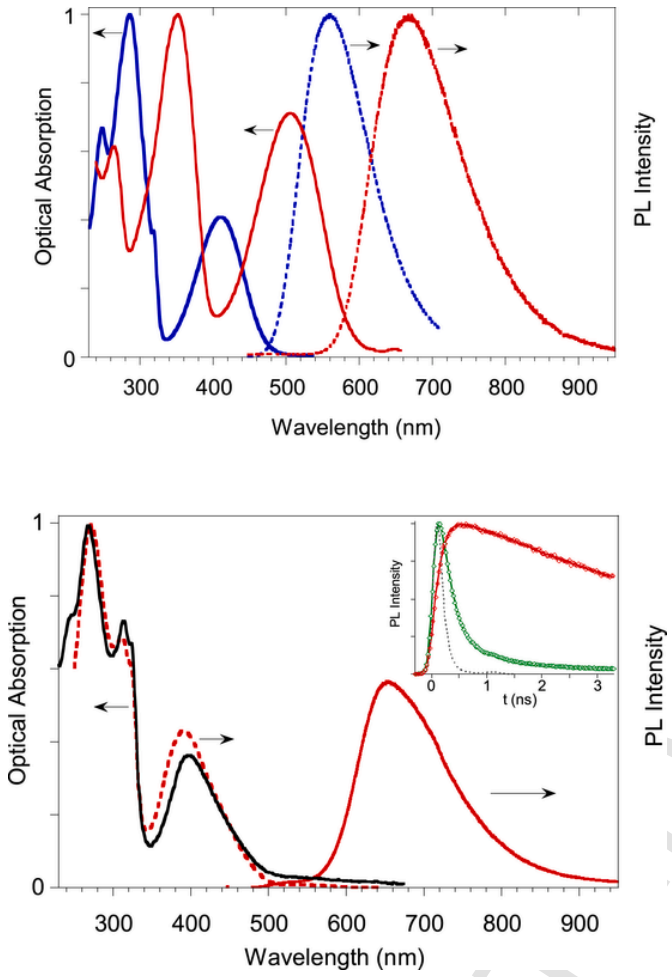

Fig. 2. Top: Normalized optical absorption (solid lines) and PL (dashed lines) spectra of chromophores **1** (blue lines) and **2** (red lines) in 10^{-4}M dichloromethane (DCM) solutions. Bottom: Normalized optical absorption (black solid line), PLE (red dotted line, λ_{em} = 655 nm) and PL (red solid line, λ_{ex} = 400 nm) spectra of **1:2** film. In the inset the PL time decay of **1:2** film (λ_{em} = 533 nm, green diamonds; λ_{em} = 650 nm, red diamonds), fits (solid lines, ESI) and prompt (grey dotted line). λ_{ex} = 408 nm.

411 nm and 508 nm, respectively. PL spectra are obtained with a NanoLog composed by a iH320 spectrograph equipped with a Synapse QExtra charge-coupled device by exciting with a monochromated 450W Xe lamp. The spectra are corrected for the instrument response. PL QY were measured with a home-made integrating sphere according to the procedure reported elsewhere [35]. Time-resolved TCSPC measurements are obtained with PPD-850 single photon detector module and DeltaTime serie DD-405L DeltaDiode Laser and analysed with the instrument Software DAS6.

Foerster Radius R_0 has been obtained from the spectroscopical properties of the molecules by [36].

$$R_0 = 0.2108\ [k^2 \bullet n^{-4} \bullet QY_D \bullet (\lambda)]^{1/6}$$

where $k = 2/3$ assuming an average orientation factor between the two transition dipoles, $n = 1.54$ is the refractive index, $Y_D = 1$ is the quantum yield of **1** and J(λ) is the overlap integral calculated as follows: $J(\lambda) = \int F_D(\lambda)\varepsilon_A(\lambda)\lambda^4 d\lambda / \int F_D(\lambda) d\lambda$ where $F_D(\lambda)$ is the fluorescence spectrum of **1** and $\varepsilon_A(\lambda)$ is the extinction molar coefficient of **2**.

Table 1
Main optical properties of the compounds. λ_{ab}, absorption maxima position; λ_{PL}, PL maximum position, τ, average PL lifetime; QY, PL Quantum Yield.

Compound	λ_{abs} (nm)	λ_{PL} (nm)	τ (ns)	QY
1 DCM	411 318, 283 247	558	11.71	0.68
1 film	400 325, 313 266	533	8.89	1
2 DCM	508 355 264	670	6.09	0.49
2 film	447 322 266	690	3.31	0.23
1:2 film	400 325, 313 266	655	6.35	0.70
3a film	408 316,307 246	546	2.26	0.21
3a:2 film	408 319,307 245	660	5.43	0.41

2.3. Morphological characterization

AFM images have been taken with a commercial AFM NT-MDT NTEGRA operating in tapping mode with cantilevers NSG10 with resonant frequency of 140–390 kHz and contact mode with cantilevers CSG10. Layer thicknesses values have been measured with AFM as the height difference between the layer top surface and the layer bottom obtained by a controlled scratch of the layer. Microscopy fluorescence images were collected with a Nikon Eclipse TE2000-U inverted confocal microscope by exciting with a 100W Hg lamp with a 450–490 nm band-pass excitation filter. Temperature dependent analysis is performed by using a Linkam LTS420 Hot-stage.

2.4. Theory and modeling

Approximation to Density Function Theory (DFT) [37] was used to model compound **1**. This approach is largely adopted for predicting structural and electronic properties of molecules (See e.g. Ref. [38] for case of molecules in complex environment). In particular we have calculated the minimum energy structure of **1**, and calculated the electronic excitation spectra and excitation dipoles via Time-Dependent DFT [39] (see Supporting Information for further details).

3. Results and discussion

3.1. Oriented thin films with polarized photoluminescence

We synthetized via Suzuki cross-coupling two rod-coil chromophores composed by a rigid backbone, (phenyl)benzo[c] [1,2,5] thiadiazole (**1**) and (phenyl)-thiophen-2-yl)benzo[c] [1,2,5]thiadiazole) (**2**) (see Scheme 1), functionalized by pentyloxy flexible chains at the head-tail positions (ESI) [40–42].

The rigid backbones possess high extinction coefficients and outstanding emission efficiencies. The flexible chains have been introduced to extend the molecules length and increase their solubility. More importantly, to increase their LC properties in order to facilitate their mechanical orientation we added alkoxy chains since it has been reported that the introduction of a polar substituent increases the dipole moment and the intermolecular interactions [5–7,43–46]. The DSC analysis of **1** evidences several thermal transitions, typical of a LC behaviour, with a thermal event at low temperature (30–45 °C, Fig. 1).

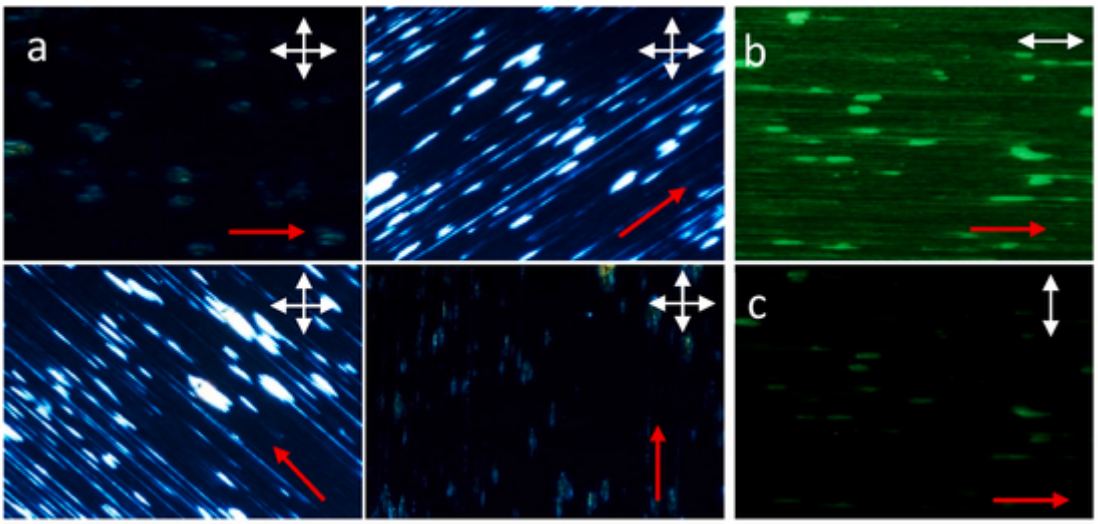

Fig. 3. Polarized optical microscopy images (POM) of a rubbed film of compound 1 obtained by 45°rotation of the film with crossed polarizers (a). Fluorescence microscopy images by excitation with blue light polarized parallel (b) or orthogonal (c) to the rubbing direction. Arrows show the polarization axis of the polarizers, red arrows show the rubbing direction, image horizontal size is 200 μm.

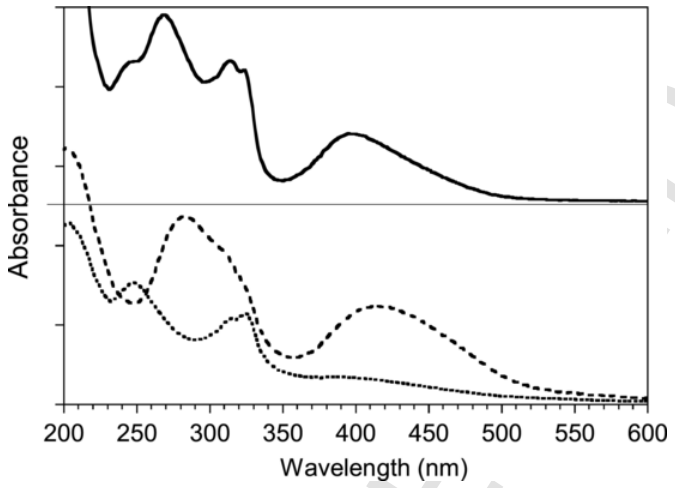

Fig. 4. Top: Absorption spectrum of a spin coated film of **1**; Bottom: Absorption spectra of an oriented film of **1** measured with light polarized parallel (dashed line) and orthogonal (dotted line) to the rubbing direction.

Conversely, molecule **2** does not display thermal events at temperatures below 100 °C (see Fig. S5b, ESI). The LC properties of **1** were further investigated by using hot-stage polarized optical microscopy (POM) (see Fig. S5a) which shows, in the first heating, the crystalline to LC transition at 106 °C, the presence of a mesophase at higher temperatures and the LC to isotropic transition at about 150 °C, in correspondence of the DSC endotherms evidenced in Fig. 1 (see inset).

Molecules **1** and **2** show high photoluminescence (PL) Quantum Yields (QY) in the green/yellow (**1**) and red (**2**) regions, both in solution and in the solid state (see Fig. 2, Fig. S11-12 and **Table 1**). Particularly interesting is compound **1** for its good film forming capability and the outstanding PL QY of the film (higher than in solution) showing an aggregation induced enhanced emission behaviour [21]. On the other hand, compound **2** is subject to aggregation quenching emission typical of thiophene based compounds [47]. In addition, its low solubility combined with a strong tendency to crystallization does not allow to produce good quality films. To obtain a red emissive film, we prepare blends of the two compounds by adding a small amount of **2** in a solution of **1**. Blended films spin-coated from solutions containing 2%w/w of **2**, hereafter called **1:2**, display absorption identical to **1** while the emission well corresponds to that of compound **2** dissolved in solution (see Fig. 2 and Table 1). This is consequence of two properties of the blend: i) the excellent compatibility of the two molecular structures that avoids micro-aggregation; ii) the efficient resonant Foerster energy transfer (FRET) [36] from **1** to **2** expected from their spectroscopic properties (theoretical Foerster radius of R_0 = 4.7 nm).

The correspondence of the PL excitation (PLE) of **1:2** with the absorption of **1** and the time resolved analysis of the emissions of **1** and **1:2** films confirm the presence of an efficient FRET from **1** to **2** through the quenching/rise of the **1**/**2** emissions in the blend (see Fig. S15, ESI and inset of Fig. 2, bottom). In addition, the PL QY of film **1:2** is higher (70%) with respect to film **2** (23%). Another advantage of the blend is to perform film orientation by mechanical methods, since the LC properties of compound **1** are fully preserved in the **1:2** blend.

To produce anisotropic films without the use of pre-aligned substrates we orient the films by mechanical rubbing (2–5 times) with a velvet cloth in order to align the rod-chain molecules along the rubbing direction (Fig. S9, ESI). The so prepared films display high optical anisotropies, as evidenced by the POM images (Fig. 3a) and by optical absorption measurements performed with polarized light (Fig. 4). The absorption spectra of oriented films of **1** display some variation with respect to the pristine film, particularly evident when measured with polarized light (see Fig. 4). The position of the lower energy absorption band (400 nm, Fig. 4 top) red-shifts to 416 nm or blue-shifts to 386 nm in the oriented film when measured with light polarized parallel or orthogonal the rubbing direction, respectively (Fig. 4 bottom). Moreover, the higher energy absorption bands, observed between 240 and 320 nm, display distinct polarizations. These features have been elucidated with the help of Density Functional calculations performed on compound **1**. In the optimized structure represented in Fig. 5 (see ESI for details), the rigid benzo[c] [1,2,5]thiadiazole core forms a dihedral angle of 39° with respect to the lateral benzene rings. The molecule length amounts to 27.7 Å. Its permanent dipole moment is 1.62 Debye, with non-zero component only along the two directions orthogonal to the long molecular axis. Adopting the optimized structure, we have calculated electronic excitations within the frame of Time-Dependent Density Functional Theory. In order to investigate the polarization of the absorption spectrum, the bands due to electronic excitation dipole moments (ETDM) parallel to the long molecular axis are reported separately from those due to ETDM orthogonal to that axis. The two most intense calculated bands, peaked at 391 and 261 nm, are polarized parallel to the long molecular axis, while the two less intense bands at 275 nm and 220 nm are polarized in the directions orthogonal to the

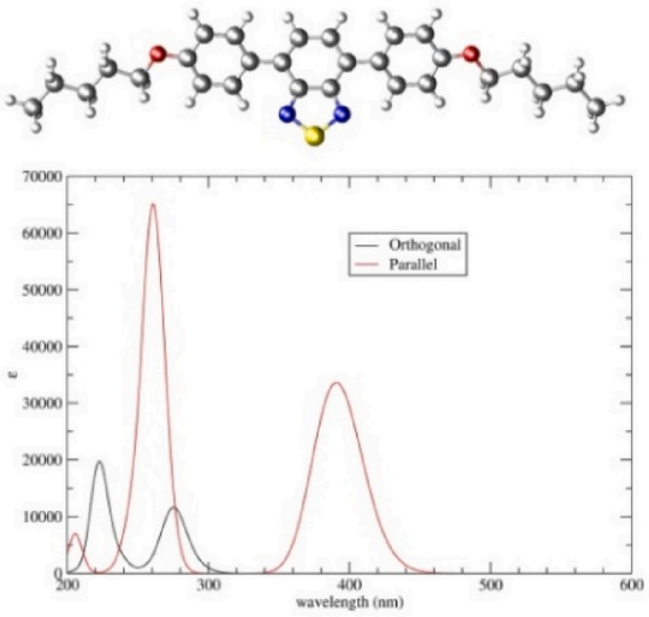

Fig. 5. Top: Ball-and-stick representation of the optimized structure of compound **1**. Atom color code: S, yellow; O, red; N, blue; C, grey; H, white. Bottom: Calculated spectrum of isolated compound **1.** Red line: excitations with ETDM parallel to the long molecular axis; black line: excitations with ETDM orthogonal with respect to the long molecular axis.

Table 2
Optical absorption and emission properties of oriented films. Absorption maxima measured with light polarized parallel (par) or orthogonal (ort) to the rubbing direction.

	λ_{abs} (par)	λ_{abs} (ort)	R_{ab}	λ_{PL}	R_{PL}
1	416	386	4.8	535	3.7
1:2	415	390	4.4	650	5.0
3a	420	396	4.3	546	5.4
3a:2	420	393	4.6	660	4.3
3b	421	396	4.6	543	5.5
3b:2	420	393	4.5	655	4.2

long axis. Relevant molecular orbitals involved in the transitions are reported in Fig. S10 (ESI). Such a finding strongly supports the anisotropy experimentally detected, moreover it also indicates how the rubbing process is capable of a successful orientation of the film. Indeed by comparing the polarized experimental spectra (Fig. 4) with the calculated ones (Fig. 5), it is possible to confirm the alignment of the long molecular axis along the rubbing direction. The polarization dependence of the lower energy absorption maximum observed experimentally (see Table 2) suggests that mechanical alignment might affect both the molecular structure and the conjugation length in the oriented film.

Our calculations help to better clarify the origin of this behaviour, already observed for oriented Poly(3-hexylthiophene) [48,49]. Indeed, the lower energy absorption band of the most elongated structure of compound **1** (optimized geometry shown in Fig. 5) is red-shifted by 15 nm with respect to a structure obtained by rotating by 90° both the terminal alcoxy chains with respect to the optimized structure (Figs. S10b and c, ESI). This finding suggests that the rubbing process, beside orienting the molecules, does contribute to their relaxation to the most stable and elongated conformation by arranging the terminal alcoxy chains, leading to a more planar structure.

The anisotropy in the absorption R_{ab} (defined as the ratio between the absorbance measured with light polarized parallel vs orthogonal to the rubbing direction) is reported in Table 2 for the lower energy absorption band (maximum value, see also Fig. 16 in ESI). Differently from the absorption, the PL spectral shape is not affected by film orientation, in fact the PL spectra measured by exciting with light parallel or orthogonal to the rubbing direction differ only in intensity. The emission anisotropy, R_{PL} (defined as the ratio between the emission intensity measured by exciting the film with light polarized parallel vs orthogonal to the rubbing direction) shows values similar to R_{ab}. (see **Table 2, Fig. 16,** ESI). The emission colours of the **1** and **1:2** films are green/yellow (533 nm) and red (650 nm), respectively (Fig. S12, ESI). The absorption spectra of the rubbed films of **1** and **1:2** evidence an increased optical diffusion after few days (Figs. S12 and S18, ESI), signature of a crystallization process induced by rubbing while pristine films do not display variations even after years. Such a behaviour is very probably related to the presence of the phase transition at 30–45°C for **1** (Fig. 1) that might produce a progressive crystallization of the film when subjected to the rubbing procedure. AFM morphological analysis of **1** and **1:2** oriented films evidences the presence of stripes induced by rubbing process (Fig. S19a and Fig. S19d) and, within each stripe, a distribution of structures with rectangular and needle-like shape associable to crystallites, for both **1** and blend **1:2** (Fig. 6a and Figs. S19e–f, respectively). Besides, a preferential orientation of the needles occurs along directions close to the orthogonality with respect to the stripe direction (for **1** see Fig.6a and Fig. S19b, this latter evidencing the orientation of the smaller needles (<1micron); for **1:2** see Fig. S19e). The needle structures of both**1** and **1:2** are partially protruding out of the stripes into the channels, determining irregular stripe edges. Even though the emission of the oriented films of **1** does not show variations, the emission of rubbed films of **1:2** display a colour change, from red to orange, after few days of storage at RT (Figs. S20 and S21, ESI), or by heating the samples at 50 °C for few minutes. Fluorescence microscopy images of these orange emitting **1:2** films evidence the presence of phase separation of the two compounds (Fig. S20, ESI), consequence of the above mentioned progressive crystallization of **1** after the rubbing procedure. This spontaneous phase separation reduces the FRET efficiency from **1** to **2** in the **1:2** films. As a consequence, the green emission from **1**, completely quenched by FRET in the **1:2** pristine film, increases in time producing the observed variation in emission colour, from red to orange.

To obtain stable red emitting oriented films, the morphological stability of compound **1** is increased by interconnecting it with non-conjugated alkyl linkers, using the approach of poly(rod-coil) polymers based on alternate definite conjugated and non-conjugated segments [50–52]. The alkyl chains are optically inactive while compound **1** acts as photoactive polymeric core assuring optical properties are retained. We interconnect the conjugated molecule **1** with long alkoxy soft linkers *via* Suzuki coupling [53–56] between 2,1,3-Benzothiadiazole-4,7-bis(boronic acid pinacol ester) and 1-bromo-4-[6-(4-bromophenoxy) hexoxy]benzene or 1-bromo-4-[12-(4-bromophenoxy)dodecoxy] benzene to give the rod-coil polymers **3a** and **3b** respectively which differ in the length of the non-conjugated alkyl segments, C6 for **3a** and C12 for **3b** (see Scheme 1 and ESI). The thermal analysis of the polymers (Figs. S6 and S7, ESI) evidences a LC behaviour that strongly depends on the length of the non-conjugated alkyl segments and the polymer molecular weight. The optical properties of the polymers in solution are identical to those of molecule **1** while the films display broader absorption bands and slightly red-shifted emission, more pronounced for the polymers with the shorter flexible chain (C6, see Table S2, ESI). The lower emission efficiency of the polymers, with respect to molecule **1**, is probably due to the presence of catalyst residues introduced during the polymerization process, as confirmed by TGA residue under air atmosphere (ca. 2 wt% for the polymers and no residue for **1**, Fig. S8) [57–59]. In Table 1 we report the results obtained with polymer **3a** displaying the higher emission efficiency. The orientation of films of polymer **3a** and **3b,** and their blends with **2**, by using the same rubbing procedure of **1** and **1:2**, produces films with similar anisotropies (see Table 2, Fig. 7, Table S2, Fig. S22) and much higher stability of the rubbed films. In fact, oriented films of **3a:2** and **3b:2** keep unchanged their red

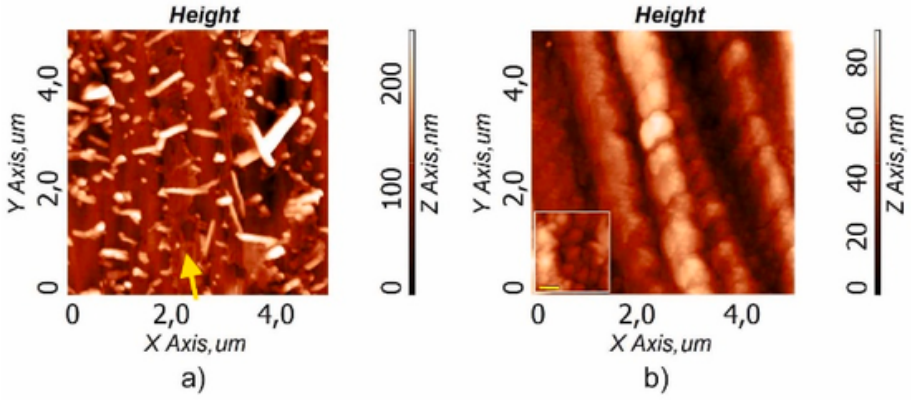

Fig. 6. AFM morphology of a) rubbed molecule **1** and b) rubbed polymer **3a** after 1 year storage. In a) the yellow arrow indicates the position and direction of a stripe induced by rubbing. In b) the inset shows the grain composition of the stripes (the thin horizontal line corresponds to 200 nm). RMS roughness:23.6 nm for a) and 15.6 nm for b).

emission and polarized optical spectra even after one year storage (Fig. S23, ESI).

The morphological analysis of the oriented films performed by AFM measurements evidences the presence of stripes with a granular and amorphous morphology both for polymer **3b** and blend **3b:2** (Fig.6b and Fig. S19l-m-n, respectively). The comparison of **3b** with **1** (see Fig. 6), shows that stripes in **3b**, instead of crystallite-like structures, totally consist of sequence of clusters of spherical grains (see inset of Fig. 6b). These results confirm the stability of the film surface that does not display formation of crystalline domains even after prolonged storage.

The significant difference between RMS of **1** and **1:2** cases (RMS: 68.4 nm and 44.0 nm, respectively) on one side and **3b** and **3b:2** (RMS: 26.2 nm and 21.0 nm, respectively) on the other side, can be explained by the distribution, in **1** and **1:2**, of crystallites with heights reaching 160 nm, induced by the rubbing process. These crystal features are not present in **3b** and **3b:2** morphologies, where more compact grain morphology occurs. (10 μm images have been chosen for all RMS values). Thickness values for rubbed layers of **1**, **1:2**, **3b** and **3b:2** are comparable with the average section height (Zav) of the corresponding layers (see Table S19b) thus suggesting that, for all the four layers, the rubbing process is likely to produce channels involving the whole layer thickness.

3.2. Mechanofluorochromism

The above mentioned peculiar properties of **1:2** films (easiness of mechanical orientation and polarized emission moving from red to orange by heating or in few days of storage at RT) can be exploited to develop highly sensitive mechanoresponsive films. In fact, even though the pristine spin-coated films of **1:2** are highly stable, after mechanical rubbing they display a spontaneous colour change, from red to orange, as a result of partial phase separation of the two compounds (Fig. 8a, Fig. S20,**S21**, ESI). The colour variation can be quantified by the CIE 1931 (x; y) chromaticity coordinates. The pristine films, as well as the as-prepared oriented films, display an emission with CIE (0.63; 0.37). After few days of storage at RT, or after heating the films at 50 °C for 5 min, the emission chromaticity coordinates of the oriented films move to CIE (0.42; 0.53). The red emission of the as-prepared oriented films can be recovered either by a further rubbing process with a velvet, or by applying a stronger mechanical stress, such as pressing and rubbing/shearing with a hand spatula (see Fig. 8, Fig. S24-27). In the first case, the mechanical rubbing is performed with the same procedure followed for the orientation of the pristine film (see Methods and ESI). The colour variation obtained by this mechanical rubbing is reversible and can be performed for several cycles (Fig.8b, Figs. S24 and S27). Differently, when the pristine red emission is recovered by a harder mechanical treatment by imprinting the film with a hand spatula, the colour variation is not fully reversible and the red emission is maintained for more than 3 months (Fig.8c, Figs. S25 and S27).

We note that the mechanofluorochromism of blend **1:2** and its reversibility is a consequence of the peculiar properties of compound **1** (see previous chapter) and is not present in the polymeric blends **3a:2** and **3b:2**. In Fig. 8 bottom, the PL spectra of a rubbed **1:2** film are compared for the freshly prepared sample (black line) and after 1 year of storage (orange line). As it can be seen from the emission profiles, the red to orange emission colour change in the aged sample is consequence of the growth of the 533 nm component (emission of compound **1**, green line) resulting from the reduced FRET efficiency. The mechanical treatment is able to re-mix the two phases that spontaneously demixed after the rubbing procedure, producing films with homogeneous red emission (Fig. S23-S27, ESI). This treatment is therefore able to reduce the average **1**–**2** inter-chromophore distance d to about 4.7 nm, activating the efficient FRET process that quenched the **1** green emission in the pristine homogeneous blend.

We would like to stress that the mechanoresponse here reported for film **1:2** is completely different from those related to a variation of the emission properties of a single molecular system, as generally encountered in organic molecules whose intra- and/or inter-molecular interactions are modulated by the external mechanical stimulus [17–30]. The mechanoresponse of the **1:2** blended film originates from the modulation of the FRET efficiency from **1** to **2**. FRET modulation induces highly sensitive chromatic changes through small variations of the inter-chromophore distances d (FRET efficiency varies as $1/d^6$). It is generally encountered in solutions, where inter-chromophore distances are varied by solvent induced aggregation, or in elastic polymeric blends, where inter-chromophore distances are modulated by mechanical forces [60,61]. In such cases the variation of d is mediated by the environment (solvent or polymer) while, in the present case, FRET modulation occurs in the bulk of the film, simplifying its preparation procedure [62].

More interestingly, the mechanical treatment with the spatula is able to orient the molecules along its direction of application (similarly to rubbing with a velvet cloth). This is evidenced by the images obtained by excitation polarized parallel or orthogonal to the direction of the spatula drawing (Figs. S25 and S26a, ESI). Therefore the peculiar de-mix/-mix properties of **1:2** blends allow to prepare films able, not only to detect a mechanical stress through an evident variation in emission colour, but also to identify the direction of application of this stress through a simple analysis with polarized light. The stability in time of the film emission colour after hard mechanical treatment with a spatula is larger than 3 months while the polarization memory is lost in about 15 days at ambient conditions. The loss of polarization memory is re-

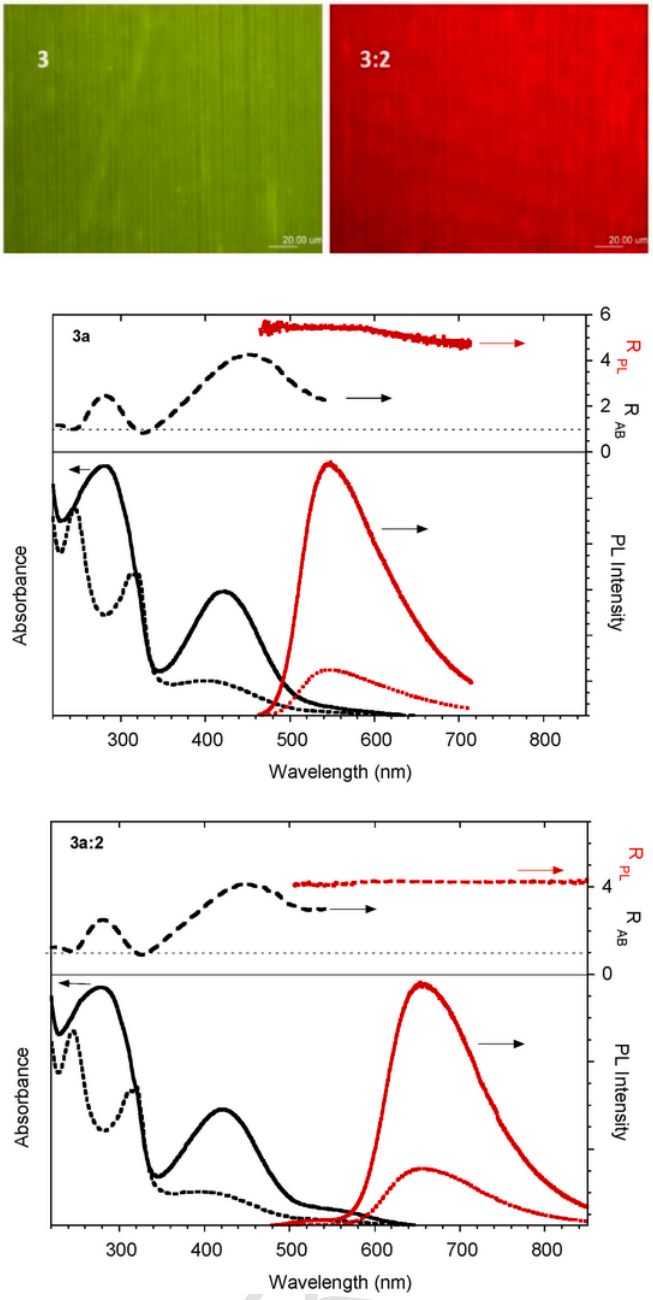

Fig. 7. Fluorescence microscopy images of rubbed films of **3a** and **3a:2** (Top). Optical properties of oriented films of **3a**(Middle) and **3a:2** (Bottom). Absorption spectra (black lines) measured with light polarized parallel (solid line) and orthogonal (dashed line) to the rubbing direction. PL spectra (red lines) excited at 400 nm with light parallel (solid line) and orthogonal (dashed line) to the rubbing direction. In the upper part of the plots the anisotropies are reported for the absorption (black line) and the emission (red line).

lated to the variation of the film morphology, that evolves from thin homogeneous film to randomly oriented needle-like crystals, whose emission polarization is orthogonal to the needle axis (see Fig. S26b).

4. Conclusion

Oriented thin films of chromophores based on rod-like rigid linear conjugated highly emissive benzothiadiazole moiety are obtained by rubbing techniques showing absorption of the two most intense bands polarized along the rubbing direction. Time-Dependent Density Functional Theory calculations show that these absorptions are polarized parallel to the long molecular axis. The red-shift of the lower energy absorption band, observed by molecular orientation, suggests that mechanical rubbing induces a conformational relaxation to the most stable and elongated state by the arrangement of the terminal alcoxy chains. Oriented films display either stable (rod-coil polymers) or mechanosensitive (molecules) emissions in the green/yellow and red regions with PL QY up to 1 and polarization ratios up to 5. The mechanoresponse of the **1:2** blended film originates from the peculiar modulation of the FRET efficiency in bulk from **1** to **2**, able to induce highly sensitive chromatic changes moving the CIE 1931 chromaticity coordinates from (0.63; 0.37) to (0.42; 0.53). The pristine red emission is either restored by further soft rubbing with a velvet cloth (reversible) or by imprinting the film with a spatula (irreversible) providing in both cases emission polarized along the rubbing direction. The peculiar properties of these blends can be exploited to prepare smart mechanical sensors able to detect the direction of application a mechanical stress through polarized emission analysis.

Author contribution statement

B. Squeo, F. Bertini, G. Scavia, M. Pasini, C. Botta, performed the experiments. F. Bertini, G. Scavia, M. Uslenghi, M. Pasini, C. Botta analyzed experimental data. E. Fois performed theoretical analysis. M. Pasini, C. Botta conceived and directed the project. M. Pasini, E. Fois, C. Botta, wrote the manuscript and all the authors contributed to manuscript revisions.

Declaration of competing interest

The authors declare that they have no known competing financial interests or personal relationships that could have appeared to influence the work reported in this paper.

Acknowledgements

This project has received funding from the ATTRACT project funded by the EC under Grant Agreement 777222. The authors wish to thank S. Incorvaia and G. Tosi for the implementation of the rubbing set-up.

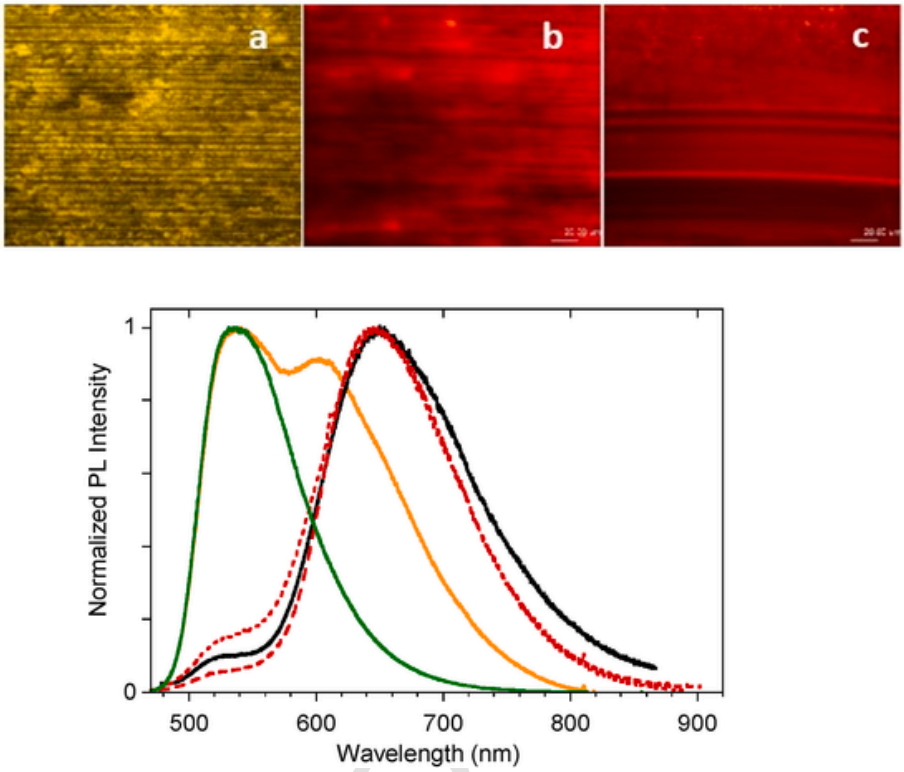

Fig. 8. Top: Fluorescence microscopy images of a rubbed **1:2** film after 1 year of storage (a), after a further rubbing treatment with velvet (b) or with a spatula (c), in the same direction of the first rubbing. Bottom: PL spectra of rubbed **1** film (green line) and **1:2** film (freshly prepared, black line; after one year storage, orange line; after a further rubbing treatment with velvet, red dashed line; after mechanical treatment with a spatula, red dotted line).

Appendix A. Supplementary data

Supplementary data to this article can be found online at https://doi.org/10.1016/j.dyepig.2022.110473.

References

[1] Weder C, Sarwa C, Montali A, Bastiaansen C, Smith P Incorporation of photoluminescent polarizers into liquid crystal displays. Science 1998;279:835–7. https://doi.org/10.1126/science.279.5352.835.

[2] Srivastava A.K, Zhang W, Schneider J, Rogach A.L, Chigrinov V.G, Kwok H.-S Photoaligned nanorod enhancement films with polarized emission for liquid-crystal-display applications. Adv Mater 2017;29:1701091. https://doi.org/10.1002/adma.201701091.

[3] Montali A, Bastiaansen C, Smith P, Weder C Polarizing energy transfer in photoluminescent materials for display applications. Nature 1998;392:261–4. https://doi.org/10.1038/32616.

[4] Menéndez-Velázquez A, Mulder C.L, Thompson N.J, Andrew T.L, Reusswig P.D, Rotschild C, et al. Light-recycling within electronic displays using deep red and near infrared photoluminescent polarizers. Energy Environ Sci 2012;6:72–5. https://doi.org/10.1039/C2EE23265K.

[5] Hirai Y, Babu S.S, Praveen V.K, Yasuda T, Ajayaghosh A, Kato T Anisotropic self-assembly of photoluminescent oligo(p-phenylenevinylene) derivatives in liquid crystals: an effective strategy for the macroscopic alignment of π-gels. Adv Mater 2009;21:4029–33. https://doi.org/10.1002/adma.200901344.

[6] Hoogboom J, Rasing T, Rowan A.E, Nolte R.J.M LCD alignment layers. Controlling nematic domain properties. J Mater Chem 2006;16:1305–14. https://doi.org/10.1039/B510579J.

[7] Wang Y, Shi J, Chen J, Zhu W, Baranoff E Recent progress in luminescent liquid crystal materials: design, properties and application for linearly polarised emission. J Mater Chem C 2015;3:7993–8005. https://doi.org/10.1039/C5TC01565K.

[8] Zhang X, Gorohmaru H, Kadowaki M, Kobayashi T, Ishi-i T, Thiemann T, et al. Benzo-2,1,3-thiadiazole-based, highly dichroic fluorescent dyes for fluorescent host–guest liquid crystal displays. J Mater Chem 2004;14:1901–4. https://doi.org/10.1039/B402645D.

[9] Ree M High performance polyimides for applications in microelectronics and flat panel displays. Macromol Res 2006;14:1–33. https://doi.org/10.1007/BF03219064.

[10] Vohra V, Anzai T Molecular orientation of conjugated polymer chains in nanostructures and thin films: review of processes and application to optoelectronics. J Nanomater 2017;2017:3624750. https://doi.org/10.1155/2017/3624750.

[11] Grell M, Bradley D.D.C, Inbasekaran M, Woo E.P A glass-forming conjugated main-chain liquid crystal polymer for polarized electroluminescence applications. Adv Mater 1997;9:798–802. https://doi.org/10.1002/adma.19970091006.

[12] Bolognesi A, Botta C, Facchinetti D, Jandke M, Kreger K, Strohriegl P, et al. Polarized electroluminescence in double-layer light-emitting diodes with perpendicularly oriented polymers. Adv Mater 2001;13:1072–5. https://doi.org/10.1002/1521-4095(200107)13:14<1072::AID-ADMA1072>3.0.CO;2-9.

[13] Sagara Y, Seki A, Kim Y, Tamaoki N Linearly polarized photoluminescence from an asymmetric cyclophane showing thermo- and mechanoresponsive luminescence. J Mater Chem C 2018;6:8453–9. https://doi.org/10.1039/C8TC02919A.

[14] Bader K, Baro A, Ehni P, Frey W, Gündemir R, Laschat S, et al. Novel luminescent diazafluorenone liquid crystals. Cryst Growth Des 2019;19:4436–52. https://doi.org/10.1021/acs.cgd.9b00211.

[15] Ryu J.-H, Lee M Liquid crystalline assembly of rod–coil molecules. In: Kato T, editor. In: Liquid crystalline functional assemblies and their supramolecular structures, vol. 128. Berlin, Heidelberg: Springer Berlin Heidelberg; 2008. p. 63–98. https://doi.org/10.1007/430_2007_061.

[16] Chen L, Zhong K.-L, Jin L.Y, Huang Z, Liu L, Hirst L.S Supramolecular honeycomb and columnar assemblies formed by self-assembly of coil-rod-coil molecules with a conjugated rod segment. Macromol Res 2010;18:800. https://doi.org/10.1007/s13233-010-0812-6. –5.

[17] Sagara Y, Kato T Stimuli-responsive luminescent liquid crystals: change of photoluminescent colors triggered by a shear-induced phase transition. Angew Chem Int Ed 2008;47:5175. https://doi.org/10.1002/anie.200800164.

[18] Yagai S, Okamura S, Nakano Y, Yamauchi M, Kishikawa K, Karatsu T, et al. Design amphiphilic dipolar π-systems for stimuli-responsive luminescent materials using metastable states. Nat Commun 2014;5:4013. https://doi.org/10.1038/ncomms5013.

[19] Huang X, Qian L, Zhou Y, Liu M, Cheng Y, Wu H Effective structural modification of traditional fluorophores to obtain organic mechanofluorochromic molecules. J Mater Chem C 2018;6:5075–96. https://doi.org/10.1039/C8TC00043C.

[20] Wang C, Li Z Molecular conformation and packing: their critical roles in the emission performance of mechanochromic fluorescence materials. Mater Chem Front 2017;1:2174–94. https://doi.org/10.1039/C7QM00201G.

[21] Zhao Z, Zhang H, Lam J.W.Y, Tang B.Z Aggregation-induced emission: new vistas at the aggregate level. Angew Chem Int Ed 2020;59:9888–907. https://doi.org/10.1002/anie.201916729.

[22] Liao R, Wang X, Peng L, Sun H, Huang W Achieving organic smart fluorophores by controlling the balance between intermolecular interactions and external stimuli. ACS Appl Mater Interfaces 2021;13:27491–9. https://doi.org/10.1021/acsami.1c07252.

[23] Botta C, Benedini S, Carlucci L, Forni A, Marinotto D, Nitti A, et al. Polymorphism-dependent aggregation induced emission of a push–pull dye and its

multi-stimuli responsive behavior. J Mater Chem C 2016;4:2979–89. https://doi.org/10.1039/C5TC03352G.
[24] Kunzelman J, Crenshaw B.R, Kinami M, Weder C Self-Assembly and dispersion of chromogenic molecules: a versatile and general approach for self-assessing polymers. Macromol Rapid Commun 2006;27:1981. https://doi.org/10.1002/marc.200600642. –7.
[25] Dai S, Zhou Y, Zhang H, Cai Z, Tong B, Shi J, et al. Turn-on and color-switchable red luminescent liquid crystals based on pyrrolopyrrole derivatives. J Mater Chem C 2020;8:11177–84. https://doi.org/10.1039/D0TC01902J.
[26] Mitani M, Ogata S, Yamane S, Yoshio M, Hasegawa M, Kato T Mechanoresponsive liquid crystals exhibiting reversible luminescent color changes at ambient temperature. J Mater Chem C 2016;4:2752–60. https://doi.org/10.1039/C5TC03578C.
[27] Zhang X, Yamaguchi R, Moriyama K, Kadowaki M, Kobayashi T, Ishi-i T, et al. Highly dichroic benzo-2,1,3-thiadiazole dyes containing five linearly π-conjugated aromatic residues, with fluorescent emission ranging from green to red, in a liquid crystal guest–host system. J Mater Chem 2006;16:736–40. https://doi.org/10.1039/B512493J.
[28] Zhu Y, Xia H, Yao L, Huang D, Song J, He H, et al. High-contrast mechanochromic benzothiadiazole derivatives based on a triphenylamine or a carbazole unit. RSC Adv 2019;9:7176–80. https://doi.org/10.1039/C9RA00141G.
[29] Gopikrishna P, Iyer P.K Monosubstituted dibenzofulvene-based luminogens: aggregation-induced emission enhancement and dual-state emission. J Phys Chem C 2016;120:26556–68. https://doi.org/10.1021/acs.jpcc.6b09689.
[30] Qian G, Wang X, Wang S, Zheng Y, Wang S, Zhu W, et al. Polymorphous luminescent materials based on 'T'-Shaped molecules bearing 4,7-Diphenylbenzo [c][1,2,5]thiadiazole skeletons: effect of substituents on the photophysical properties. Chem Eur J 2019;25:15401–10. https://doi.org/10.1002/chem.201904026.
[31] Li H.-J, Wang J.-T, Mei C.-Y, Li W.-S A new class of organic photovoltaic materials: poly(rod-coil) polymers having alternative conjugated and non-conjugated segments. Chem Commun 2014;50:7720–2. https://doi.org/10.1039/C4CC03409K.
[32] Lee D.H, Lee J.H, Kim H.J, Choi S, Park G.E, Cho M.J, et al. n–σ–(A)m type partially conjugated block copolymer and its performance in single-component polymer solar cells. J Mater Chem 2017;5:9745–51. https://doi.org/10.1039/C7TA01819C.
[33] Kazerouni N, Melenbrink E.L, Das P, Thompson B.C Ternary blend organic solar cells incorporating ductile conjugated polymers with conjugation break spacers. ACS Appl Polym Mater 2021;3:3028–37. https://doi.org/10.1021/acsapm.1c00213.
[34] Shao W, Liang L, Xiang X, Li H, Zhao F, Li W Changing to poly(rod-coil) polymers: a promising way for an optoelectronic compound to improve its film formation. Chin J Chem 2015;33:847–51. https://doi.org/10.1002/cjoc.201500179.
[35] Moreau J, Giovanella U, Bombenger J.-P, Porzio W, Vohra V, Spadacini L, et al. Highly emissive nanostructured thin films of organic host–guests for energy conversion. ChemPhysChem 2009;10:647–53. https://doi.org/10.1002/cphc.200800682.
[36] Lakowicz J.R Principles of fluorescence spectroscopy. New York: Kluwer Academic Plenum Publishers; 1999.
[37] Chai J.-D, Head-Gordon M Long-range corrected hybrid density functionals with damped atom–atom dispersion corrections. Phys Chem Chem Phys 2008;10:6615–20. https://doi.org/10.1039/B810189B.
[38] Zhou X, Wesolowski T.A, Tabacchi G, Fois E, Calzaferri G, Devaux A First-principles simulation of the absorption bands of fluorenone in zeolite L. Phys Chem Chem Phys 2012;15:159–67. https://doi.org/10.1039/C2CP42750H.
[39] Casida M.E, Jamorski C, Casida K.C, Salahub D.R Molecular excitation energies to high-lying bound states from time-dependent density-functional response theory: characterization and correction of the time-dependent local density approximation ionization threshold. J Chem Phys 1998;108:4439–49. https://doi.org/10.1063/1.475855.
[40] Botta C, Betti P, Pasini M Organic nanostructured host–guest materials for luminescent solar concentrators. J Mater Chem 2012;1:510–4. https://doi.org/10.1039/C2TA00632D.
[41] Giovanella U, Betti P, Bolognesi A, Destri S, Melucci M, Pasini M, et al. Core-type polyfluorene-based copolymers for low-cost light-emitting technologies. Org Electron 2010;11:2012. https://doi.org/10.1016/j.orgel.2010.09.009. –8.
[42] Cappelli A, Villafiorita-Monteleone F, Grisci G, Paolino M, Razzano V, Fabio G, et al. Highly emissive supramolecular assemblies based on π-stacked polybenzofulvene hosts and a benzothiadiazole guest. J Mater Chem C 2014;2:7897–905. https://doi.org/10.1039/C4TC01200C.
[43] Ahmed H.A, Hagar M, Aljuhani A Mesophase behavior of new linear supramolecular hydrogen-bonding complexes. RSC Adv 2018;8:34937–46. https://doi.org/10.1039/C8RA07692H.
[44] Ahmed H.A, Naoum M.M, Saad G.R Mesophase behaviour of 1:1 mixtures of 4-n-alkoxyphenylazo benzoic acids bearing terminal alkoxy groups of different chain lengths. Liq Cryst 2016;43:1259–67. https://doi.org/10.1080/02678292.2016.1166528.
[45] Alnoman R, Al-Nazawi F.K, Ahmed H.A, Hagar M Synthesis, optical, and geometrical approaches of new natural fatty acids' esters/schiff base liquid crystals. Molecules 2019;24:4293. https://doi.org/10.3390/molecules24234293.
[46] Qiu B, Chen S, Xue L, Sun C, Li X, Zhang Z.-G, et al. Effects of alkoxy and fluorine atom substitution of donor molecules on the morphology and photovoltaic performance of all small molecule organic solar cells. Front Chem 2018;6. https://doi.org/10.3389/fchem.2018.00413.
[47] Botta C, Patrinoiu G, Picouet P, Yunus S, Communal J.-E, Cordella F, et al. Organic nanostructured host–guest materials containing three dyes. Adv Mater 2004;16:1716–21. https://doi.org/10.1002/adma.200400200.
[48] Kajiya D, Ozawa S, Koganezawa T, Saitow K Enhancement of out-of-plane mobility in P3HT film by rubbing: aggregation and planarity enhanced with low regioregularity. J Phys Chem C 2015;119:7987–95. https://doi.org/10.1021/jp510675r.
[49] Bolognesi A, Botta C, Martinelli M, Porzio W Polarized photoluminescence and electroluminescence in oriented films of regioregular poly(3-alkylthiophenes). Org Electron 2000;1:27–32. https://doi.org/10.1016/S1566-1199(00)00005-7.
[50] Shao W, Liang L, Xiang X, Li H, Zhao F, Li W Changing to poly(rod-coil) polymers: a promising way for an optoelectronic compound to improve its film formation. Chin J Chem 2015;33:847–51. https://doi.org/10.1002/cjoc.201500179.
[51] Xiao W.-J, Wang J, Li H.-J, Liang L, Xiang X, Chen X.-Q, et al. Interconnecting semiconducting molecules with non-conjugated soft linkers: a way to improve film formation quality without sacrifice in charge mobility. RSC Adv 2018;8:23546–54. https://doi.org/10.1039/C8RA04405H.
[52] Li H.-J, Wang J.-T, Mei C.-Y, Li W.-S A new class of organic photovoltaic materials: poly(rod-coil) polymers having alternative conjugated and non-conjugated segments. Chem Commun 2014;50:7720–2. https://doi.org/10.1039/C4CC03409K.
[53] Pasini M, Destri S, Porzio W, Botta C, Giovanella U Electroluminescent poly (fluorene-co-thiophene-S,S-dioxide): synthesis, characterisation and structure–property relationships. J Mater Chem 2003;13:807–13. https://doi.org/10.1039/B208742A.
[54] Giovanella U, Botta C, Galeotti F, Vercelli B, Battiato S, Pasini M Perfluorinated polymer with unexpectedly efficient deep blue electroluminescence for full-colour OLED displays and light therapy applications. J Mater Chem C 2013;1:5322–9. https://doi.org/10.1039/C3TC31139B.
[55] Bolognesi A, Betti P, Botta C, Destri S, Giovanella U, Moreau J, et al. From block copolymers to end-capped polymers: a suitable method to control the electro-optical properties of polymeric materials. Macromolecules 2009;42:1107–13. https://doi.org/10.1021/ma802587f.
[56] Squeo B.M, Carulli F, Lassi E, Galeotti F, Giovanella U, Luzzati S, et al. Benzothiadiazole-based conjugated polyelectrolytes for interfacial engineering in optoelectronic devices. Pure Appl Chem 2019;91:477–88. https://doi.org/10.1515/pac-2018-0925.
[57] Sakamoto J, Rehahn M, Wegner G, Schlüter A.D Suzuki Polycondensation: polyarylenes à la Carte. Macromol Rapid Commun 2009;30:653–87. https://doi.org/10.1002/marc.200900063.
[58] Camaioni N, Tinti F, Franco L, Fabris M, Toffoletti A, Ruzzi M, et al. Effect of residual catalyst on solar cells made of a fluorene-thiophene-benzothiadiazole copolymer as electron-donor: a combined electrical and photophysical study. Org Electron 2012;13:550–9. https://doi.org/10.1016/j.orgel.2011.12.005.
[59] Krebs F.C, Nyberg R.B, Jørgensen M Influence of residual catalyst on the properties of conjugated polyphenylenevinylene materials: palladium nanoparticles and poor electrical performance. Chem Mater 2004;16:1313–8. https://doi.org/10.1021/cm035205w.
[60] Villafiorita-Monteleone F, Cappelli A, Paolino M, Colombo M, Cariati E, Mura A, et al. Aggregation-induced förster resonance energy transfer in polybenzofulvene/dye nanoparticles. J Phys Chem C 2015;119:18986–91. https://doi.org/10.1021/acs.jpcc.5b05589.
[61] Morgner F, Bennemann M, Cywiński P.J, Kollosche M, Górski K, Pietraszkiewicz M, et al. Elastic FRET sensors for contactless pressure measurement. RSC Adv 2017;7:50578–83. https://doi.org/10.1039/C7RA06379B.
[62] Ma Z, Ji Y, Wang Z, Kuang G, Jia X Mechanically controlled FRET to achieve an independent three color switch. J Mater Chem C 2016;4:10914–8. https://doi.org/10.1039/C6TC04168J.